Thermochemical Mechanism Optimization for Accurate Predictions of CH Concentrations in Premixed Flames of C_1-C_3 Alkane Fuels

Philippe Versailles
Postdoctoral Researcher, ASME Member
Department of Mechanical Engineering
McGill University
Montréal, Québec, H3A 0C3
Canada
philippe.versailles@mail.mcgill.ca

Graeme M.G. Watson
Combustion Engineer
Siemens Canada Limited
Montréal, Québec H9P 1A5
Canada
graeme.watson@siemens.com

Antoine Durocher
PhD Student, ASME Student Member
Department of Mechanical Engineering
McGill University
Montréal, Québec, H3A 0C3
Canada
antoine.durocher@mail.mcgill.ca

Gilles Bourque
Combustion Key Expert, ASME Fellow
Siemens Canada Limited
Montréal, Québec H9P 1A5
Canada
gilles.bourque@siemens.com

Adjunct Professor
Department of Mechanical Engineering
McGill University
Montréal, Québec, H3A 0C3
Canada
gilles.bourque@mcgill.ca

Jeffrey M. Bergthorson[*]
Associate Professor, ASME Member
Department of Mechanical Engineering
McGill University
Montréal, Québec, H3A 0C3
Canada
jeff.bergthorson@mcgill.ca

Increasingly stringent regulations on NO_x emissions are enforced by governments owing to their contribution in the formation of ozone, smog, fine aerosols, acid rains and nutrient pollution of surface water, which affect human health and environment. The design of high-efficiency, low-emission combustors achieving these ever-decreasing emission standards requires thermochemical mechanisms of sufficiently high accuracy. Recently, a comprehensive set of experimental data, collected through laser-based diagnostics in atmospheric, jet-wall, stagnation, premixed flames, was published for all isomers of C_1-C_4 alkane and alcohol fuels [1–3]. The rapid formation of NO through the flame front via the prompt (Fenimore) route was shown to be strongly coupled to the maximum concentration of the methylidyne radical, $[CH]_{peak}$, and the flow residence time within the CH layer. A proper description of CH formation is then a prerequisite for accurate predictions of NO concentrations in hydrocarbon-air flames. However, a comparison against the Laser-Induced Fluorescence (LIF) experimental data of [3] revealed that 1) modern thermochemical mechanisms are unable to accurately capture the stoichiometric dependence of $[CH]_{peak}$, and 2) for a given equivalence ratio, the predictions of different mechanisms span over more than an or-

[*]Corresponding author. Email: jeff.bergthorson@mcgill.ca

der of magnitude. This paper presents an optimization of the specific rate of a selection of nine elementary reactions included in the San Diego combustion mechanism [4]. A quasi-Newton algorithm is used to minimize an objective function defined as the sum of squares of the relative difference between the numerical and experimental CH-*LIF data of [3], while constraining the specific rates to physically reasonable values. A mechanism properly describing* CH *formation for lean to rich,* C_1-C_3 *alkane-air flames is obtained. This optimized mechanism will enable accurate predictions of prompt-*NO *formation over a wide range of equivalence ratios and alkane fuels. Suggestions regarding which reactions require further investigations, either through experimental or theoretical assessments of the individual specific rates, are also provided.*

Nomenclature
Thermochemical mechanisms

SD   San Diego, version 2005 [4]
GRI   GRI-Mech 3.0 [5]
USC   USC Mech II [6]
NUIG1   Aramco Mech 1.3 [7]
NUIG2   Aramco Mech 2.0 [8]
KON   Konnov, revision 0.6 [9]

1 Introduction

Nitric oxide, NO, is a primary pollutant produced by the oxidation of nitrogen, mainly in combustion-based applications. In the atmosphere, NO is rapidly oxidized to NO_2, leading to the formation of ground-level ozone, acid precipitations, fine particulate matter, and nutrient pollution that affect human health and environment [10, 11]. Four NO formation pathways are recognized in the combustion of gaseous flames: thermal (Zel'dovich), prompt (Fenimore), N_2O, and NNH [12, 13]. The prompt route, initiated by the reaction $CH + N_2 \leftrightarrow NCN + H$, is responsible for the rapid production of NO within the front of hydrocarbon flames. Recently, Watson and co-workers [2] reported a series of experimental velocity, NO and CH concentration profiles measured in atmospheric-pressure, rich ($\phi = 1.3$), premixed, jet-wall stagnation flames of pure C_1-C_4 alkane and alcohol fuels mixed with air. They demonstrated a strong, linear correlation between the formation of prompt-NO and the maximum concentration of the methylidyne radical, $[CH]_{peak}$, scaled by the residence time in the CH layer, τ_{CH}, defined as the ratio of the width of the CH layer taken at half-maximum and the strained reference flame speed. These results confirm methylidyne as the primary precursor of prompt-NO formation in premixed flames, and put the prerequisite for kinetic mechanisms to accurately predict the CH layer profile in order to properly describe NO production.

Using Laser-Induced Fluorescence (LIF), Versailles and co-workers [3] reported quantitative $[CH]_{peak}$ values measured in premixed, jet-wall stagnation flames of C_1-C_4 normal alkanes at equivalence ratios, ϕ, ranging from 0.7 to 1.5. For all fuels, the maximum CH-LIF signal, a surrogate measure of

$[CH]_{peak}$, is maximized at an equivalence ratio of 1.2 and decreases monotonically as the stoichiometry is shifted to leaner and richer mixtures. The consistency of this behavior for all considered alkanes suggests that CH formation is determined by fuel-independent elementary reactions. A benchmarking of four thermochemical mechanisms [4–7] against the experimental data revealed two significant deficiencies. First, variations of more than an order of magnitude in the predicted CH concentrations by the various models were observed and tracked, using reaction path and sensitivity analyses, to significant differences in terms of the rate coefficients and reactions involved in the CH formation route ($CH_3 \rightarrow CH_2^* \rightarrow CH_2 \rightarrow CH$) and removing carbon atoms from the CH formation route (principally via CH consumption). Second, the mechanisms overestimate the decline in $[CH]_{peak}$ as the mixture is shifted to lean mixtures from the maximum CH concentration occurring at $\phi = 1.2$. This behavior was also observed in [14, 15] for a set of kinetic mechanisms [4, 5, 16, 17], but the exact source and possible remedy remain to be determined. Considering the correlation reported in [2], these inconsistencies impact the ability of thermochemical mechanisms to accurately predict prompt-NO formation.

The current paper aims to diagnose the source of the improper variation of $[CH]_{peak}$ with ϕ, as well as to highlight the reactions requiring an improved specification of their rate coefficients. An optimization procedure is applied to the San Diego mechanism [4], which displayed the best overall predictive performance in the analysis of Versailles and co-workers [3], while at the same time including the fewest number of species and elementary reactions. The pre-exponential factors of nine elementary reactions, interacting with the CH formation route and selected via sensitivity analyses, are adjusted to yield a thermochemical mechanism that agrees, within uncertainty, with the CH-LIF experimental data presented in [3].

2 Methodology

The optimization procedure used here is inspired by [2,18]. It consists in adjusting the specific rate of a subset of the elementary reactions included in the thermochemical mechanism to reconcile numerical predictions against a selection of experimental data points. As discussed in Appendix A, the uncertainty in the thermodynamic properties is negligible in comparison to the contribution of the uncertain rate coefficients to the error on $[CH]_{peak}$ predictions and, therefore, only the kinetic parameters are considered in the optimization.

For bimolecular reactions, the specific rate is defined as $k(T) = A \cdot T^n \cdot \exp(-E_a/R_u T)$, where A is the pre-exponential factor, n the temperature exponent, and E_a the activation energy. Even more parameters are required to describe the specific rate of pressure-dependent, uni-molecular reactions [19]. As discussed in [3] and revealed by the sensitivity analyses presented below (see Fig.1), the stoichiometric dependence of $[CH]_{peak}$ for all fuels is determined by a limited number of fuel-independent elementary reactions. This implies that the 25 data points for the C_1-C_3 alkane-air flames presented in [3] are not independent, and including all rate coefficients (A, n, and E_a) for all

reactions of interest would lead to an ill-resolved optimization problem. This limitation could be alleviated by considering additional, independent experimental data. However, to the best knowledge of the authors, the measurements of Versailles and co-workers [3] are the only currently available absolute CH concentration measurements for atmospheric-pressure flames over a range of equivalence ratios. Therefore, as in [2, 18], only the pre-exponential factor of select reactions is adjusted in the current optimization. The procedure seeks to minimize the objective function, F, defined as the sum of squares of the relative difference between the numerical and experimental data, $(S_{LIF}/S_R)_{num,j}$ and $(S_{LIF}/S_R)_{exp,j}$, respectively:

$$F(\vec{A}) = \sum_j \left[\frac{(S_{LIF}/S_R)_{num,j}(\vec{A}) - (S_{LIF}/S_R)_{exp,j}}{(S_{LIF}/S_R)_{exp,j}} \right]^2, \quad (1)$$

where the summation is performed for a set of experimental optimization targets j, and the dependence of the objective function and numerical LIF signals to the pre-exponential factors is shown in vectorial notation as $\vec{A}$.

Versailles and co-workers [3] employed the comparative diagnostic approach [20] where numerical signal intensities, generated by post-processing flame solutions using a LIF model, are directly compared to relatively raw experimental data. This method separates computations and experiments; the uncertainties in the assumed temperature and species concentration profiles required in the LIF model do not reflect in the experimental data and, even if the LIF model eventually becomes obsolete, the experimental data remain relevant and accurate. The numerical CH-LIF signal (S_{LIF}) is obtained by using a time-resolved, four-level LIF model, and is normalized by the Rayleigh scattering signal of pure nitrogen (S_R) to calibrate for the transmissivity and efficiency of the collection optics and camera, thus making S_{LIF}/S_R a quantitative, surrogate measure of [CH]. Details of the experimental method and LIF modeling, as well as estimated concentrations in parts per million, are provided in [3].

The first step of the optimization is to identify the active parameters, which are the pre-exponential factors of the reactions that have the greatest influence on $[CH]_{peak}$, while at the same time featuring a relatively large uncertainty in their specific rate description. Second, bounds on the active parameters are determined to ensure that the pre-exponential factors remain within a range of physically reasonable values. Then, a selection of experimental data points is made to serve as optimization targets, and a quasi-Newton optimization method is applied to yield the vector $\vec{A}$ that minimizes the function F.

2.1 Identification of the active parameters

Figure 1 presents the logarithmic sensitivity of the maximum CH mole fraction ($X_{CH,peak}$) to the specific rate of individual reactions i, L.S. $(X_{CH,peak}, i)$, obtained from the solutions of stagnation flames computed with Chemkin-Pro [21]. The experimental boundary conditions for the 25 C₁-C₃ alkane-air flames are provided in [3]. The reactions are sorted according to the

sum of squares of L.S. $(X_{CH,peak}, i)$ for all considered flames, and only the 20 most important reactions are shown for the sake of brevity. For each reaction, the bands of the sensitivity plots are colored according to the equivalence ratio using a blue ($\phi = 0.7$) to red ($\phi = 1.5$) rainbow colormap.

The overprediction of the decline in $[CH]_{peak}$ as the stoichiometry is shifted to lean mixtures from $\phi = 1.2$ must be related to 1) an overestimation of the specific rate of reactions with increasing values of L.S. $(X_{CH,peak}, i)$ with ϕ, e.g., $CH + O_2 \leftrightarrow HCO + O$ or $CH_2 + O_2 \leftrightarrow CO + OH + H$, 2) an underestimation of $k(T)$ for reactions with decreasing values of L.S. $(X_{CH,peak}, i)$ with ϕ, e.g., $CH_3 + OH \leftrightarrow CH_2^* + H_2O$ or $CH + H_2O \leftrightarrow CH_2O + H$, or 3) a combination of both. Many reactions in Fig.1 present the expected relationship between L.S. $(X_{CH,peak}, i)$ and ϕ, and/or feature significant values of logarithmic sensitivities. However, not all reactions are known to the same level of certainty. As discussed in [3], the specific rates of the reactions interacting with the CH formation route are not consistent among thermochemical mechanisms while, in contrast, there is a relatively well-established consensus regarding $k(T)$ for the principal reactions in the H_2/O_2 sub-mechanism, CO to CO_2 conversion, and main fuel breakdown route. As suggested in [18], the uncertainty in the specific rate of the individual reactions must also be taken into account in the selection of the active parameters; they must have a significant impact on $[CH]_{peak}$, while at the same time allowing a sufficiently wide adjustment to reconcile the numerical and experimental data.

Figure 2 presents the product of L.S. $(X_{CH,peak}, i)$ with the relative error in the specific rate of reaction i, $\Delta k_i/k_i$. The uncertainty in k_i is generally provided as $\Delta \log_{10} k_i$, and the lower and upper bounds of the specific rate obtained by division and multiplication, respectively, of k_i by the factor $f_i = 10^{\Delta \log_{10} k_i}$ [22,23]. It follows that the lower and upper limits of relative error are:

$$\left. \frac{\Delta k_i}{k_i} \right|_{low} = \frac{k_i/f_i - k_i}{k_i} = \frac{1}{f_i} - 1, \quad (2)$$

and

$$\left. \frac{\Delta k_i}{k_i} \right|_{high} = \frac{k_i \cdot f_i - k_i}{k_i} = f_i - 1, \quad (3)$$

respectively. Values of $\left. \frac{\Delta k_i}{k_i} \right|_{high}$ obtained from [22, 24] are used in Fig.2.

As observed in Fig.2, only a subset of the reactions combines high values of L.S. $(X_{CH,peak}, i)$ and $\Delta k_i/k_i$, thus making their pre-exponential factor a suitable candidate as an active parameter. The 9 reactions included in the optimization are shown in boldface. They interact with the CH formation route by consuming or producing methylidyne or its precursors, and were observed in the course of the work to have a limited impact on global combustion properties, such as the strained reference flame speed. Reactions from the H_2/O_2 sub-mechanism,
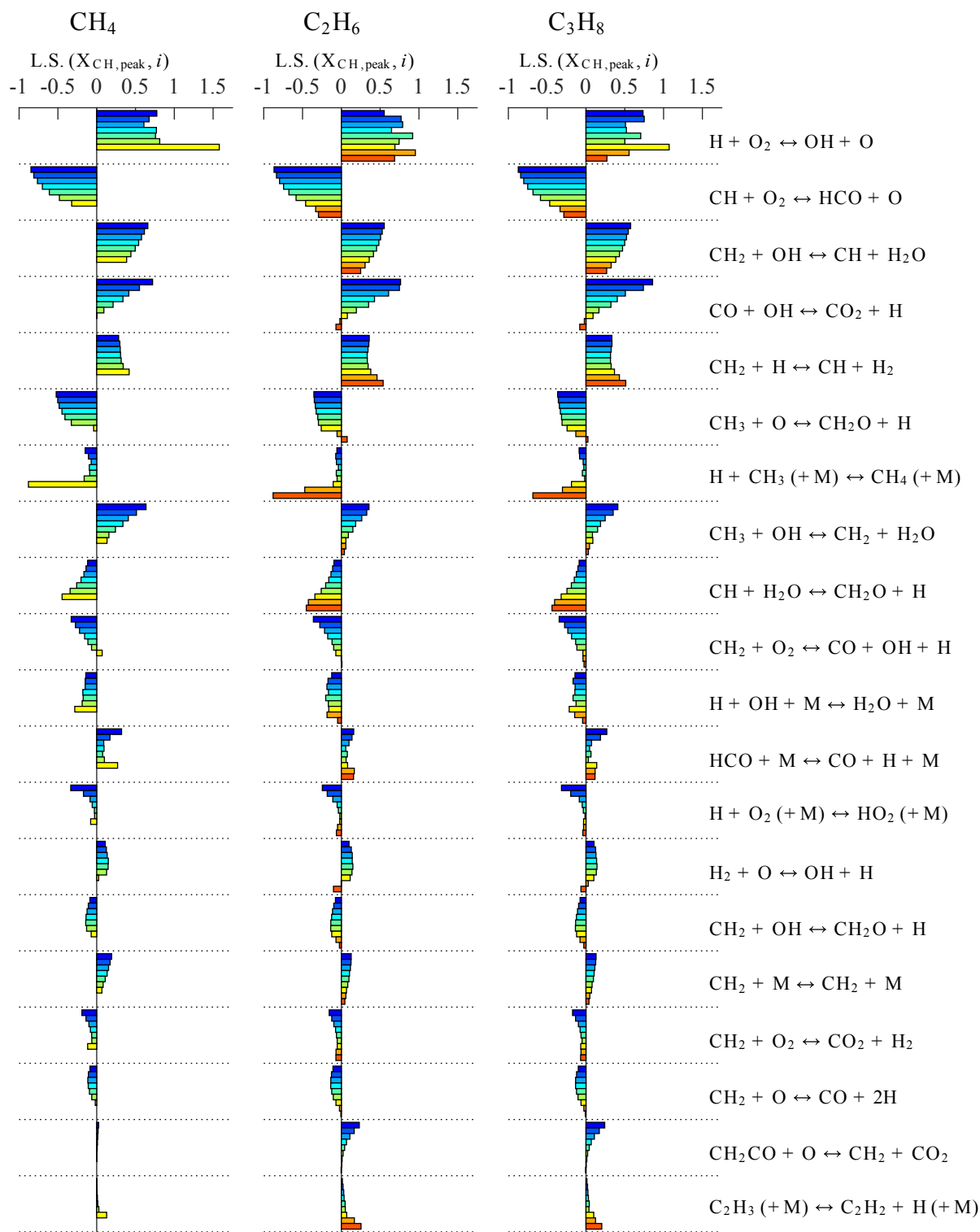

Fig. 1. Logarithmic sensitivity of the maximum CH mole fraction to the specific rate of individual reactions, $\text{L.S.}\left(X_{\text{CH,peak}}, i\right)$. The reactions are sorted in decreasing order of $\sum\limits_{C_mH_n,\phi} \text{L.S.}\left(X_{\text{CH,peak}}, i\right)^2$. For each reaction, the bands are colored according to a blue ($\phi = 0.7$) to red ($\phi = 1.5$) rainbow colormap.

namely $H + O_2 \leftrightarrow OH + O$, are not considered in the optimization as their specific rates can be, and were, benchmarked

against experiments providing a significantly higher level of accuracy than the experimental data in [3], e.g., flame speed or
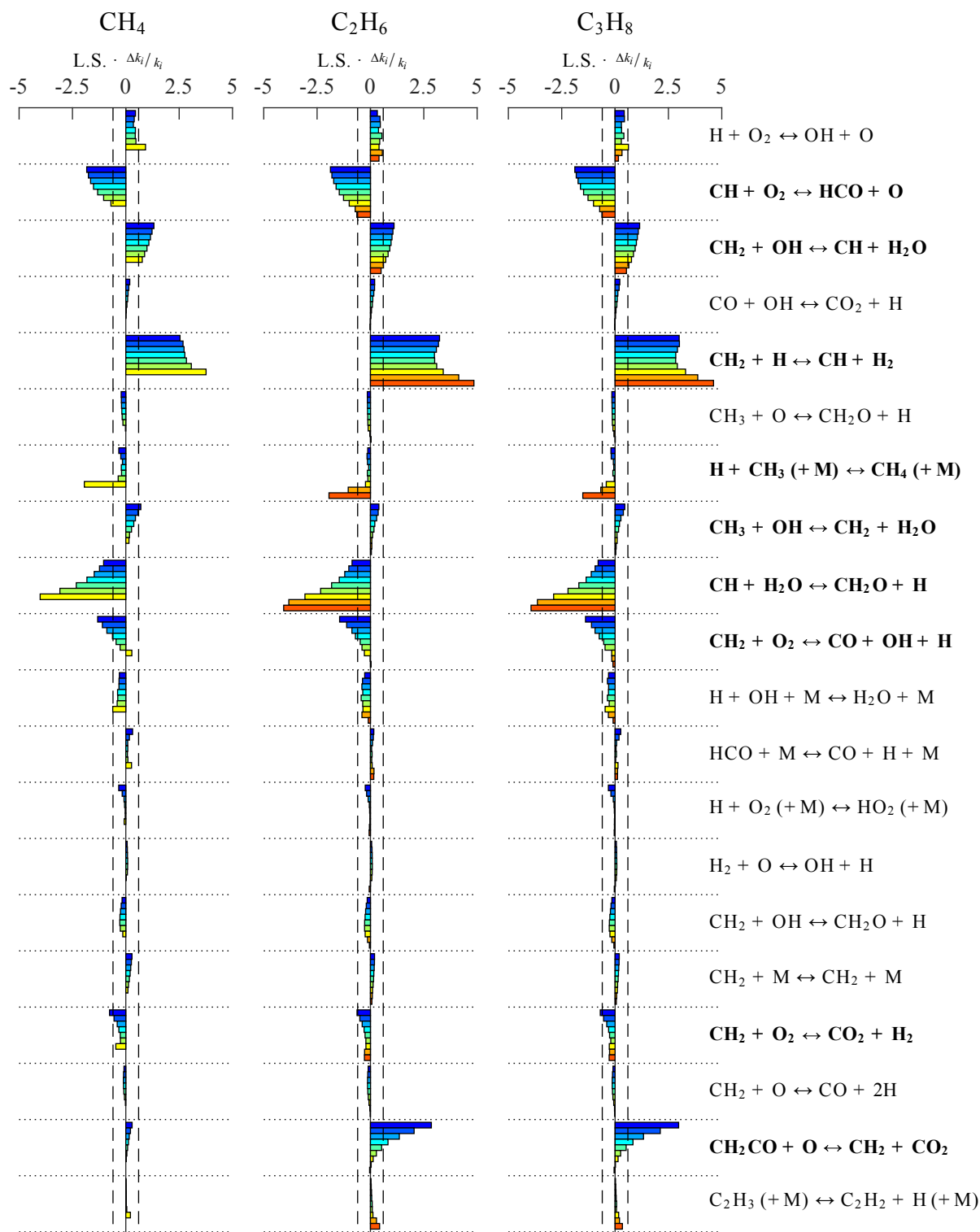
Fig. 2.   Product of L.S. $\left(X_{\mathrm{CH,peak}}, i\right)$ with $^{\Delta k_i}/_{k_i}$. The relative errors are obtained from the upper uncertainty limits estimated in [22, 24]. The black, dashed lines correspond to L.S. $\left(X_{\mathrm{CH,peak}}, i\right) \cdot {}^{\Delta k_i}/_{k_i} = \pm 0.6$.

ignition delay time measurements [5, 7], and the thermochemical mechanisms provide consistent descriptions of $k(T)$.

2.2   Bounds on the value of the active parameters

Bounds for the active parameters must be determined to restrict the specific rates to physically realistic values [18], but they must be sufficiently broad to allow the optimization pro-

Table 1.   Lower and upper optimization bounds, $1/f_{i,\text{low}}$ and $f_{i,\text{high}}$, respectively.

Reactions	Bounds[1]	
	$1/f_{i,\text{low}}$	$f_{i,\text{high}}$
$CH + O_2 \leftrightarrow HCO + O$	0.4747	2.456
$CH_2 + OH \leftrightarrow CH + H_2O$	0.2409	2.168
$CH_2 + H \leftrightarrow CH + H_2$	0.7579	127.6
$H + CH_3 (+M) \leftrightarrow CH_4 (+M)$	0.2577	3.246
$CH_3 + OH \leftrightarrow CH_2^* + H_2O$	0.3653	2.324
$CH + H_2O \leftrightarrow CH_2O + H$	$3.823 \cdot 10^{-2}$	5.295
$CH_2 + O_2 \leftrightarrow CO + OH + H$ $\leftrightarrow CO_2 + H_2$	0.8482	8.482
$CH_2CO + O \leftrightarrow CH_2 + CO_2$	$5.808 \cdot 10^{-3}$	1.502

Table 2.   Experimental optimization targets, $(S_{\text{LIF}}/S_R)_{\text{exp},i}$ [3].

φ	0.7	0.8	0.9	1.0	1.1	1.2	1.3	1.4	1.5
CH_4			5.8			16.5	11.9		
C_2H_6	1.8			13.0					5.5
C_3H_8		5.5			24.8		23.2		6.0

cedure to converge to an accurate thermochemical mechanism. Lower and upper multiplier values, $f_{i,\text{low}}$ and $f_{i,\text{high}}$, respectively, for the pre-exponential factor of each reaction are reported in Table 1. As presented in Appendix B, they are determined through comparison of the specific rates included in the SD mechanism to Arrhenius rate coefficients available in the literature. During the optimization, the pre-exponential factor of a given reaction i is allowed to take any value between $A_i/f_{i,\text{low}}$ and $A_i \cdot f_{i,\text{high}}$, where A_i is the original pre-exponential factor. It is noted that the reactions $CH_2 + O_2 \leftrightarrow CO + OH + H$ and $CH_2 + O_2 \leftrightarrow CO_2 + H_2$ are optimized together and, therefore, the same multiplier applies to both to maintain the branching among the product channels.

2.3   Experimental optimization targets

In a classical optimization, the number of degrees of freedom, n_{DOF}, which is the difference between the number of optimization targets, $(S_{\text{LIF}}/S_R)_{\text{exp},i}$, and the number of adjustable parameters, the pre-exponential factors of the reactions identified above, must be positive [18]. Other constraints, such as the restriction of the optimization space by the bounds $f_{i,\text{low}}$ and $f_{i,\text{high}}$, and implicit constraints within the chemical mechanism (e.g., mass balances), increase n_{DOF} [18]. On the other hand, as discussed previously, the experimental data points are not independent as they are determined by a common set of elementary reactions. Practically, this reduces n_{DOF}, and implies that including all experimental data points would not result in a corresponding increase in n_{DOF}. In the current optimization, 10 experimental targets are selected to adjust 8 pre-exponential factors, yielding $n_{\text{DOF}} = 2$ when excluding the implicit factors discussed above. As reported in [18], the exact determination of n_{DOF} is difficult, and beyond the scope of this paper. The experimental data considered in the optimization, presented in Table 2, encompass the whole range of fuels and equivalence

ratios in an attempt to properly capture the impact of the alkane chain-length and stoichiometry on the response of the model.

2.4   Optimization algorithm

Minimization of the function $F(\vec{A})$, defined in equation (1), is performed using the constrained, non-linear, quasi-Newton, multi-variate algorithm (fmincon) of Matlab (version R2015b). Flame simulations are solved at each iteration of the optimization and processed into numerical LIF signals, $(S_{\text{LIF}}/S_R)_{\text{num},i}$, using the time-resolved, four-level CH-LIF model presented in [3,25]. Matlab not only solves the optimization problem, it also manages the flame simulations by updating the thermochemical mechanism with the new pre-exponential factors, launching the jet-wall, stagnation flame solver of Cantera 2.2.1 [26] through Python 3.4, and converting the flame solutions to LIF signals. As relatively small changes in $\vec{A}$ are specified by the algorithm, the flame solver uses the solutions from the previous optimization iteration as initial guesses to accelerate the computations.

3   Comparison of optimized mechanisms to the experimental data

Tables 3 and 4 present two solutions obtained with the optimization method. The multiplier values $f_{i,\text{orig}}$, yielding an objective function $F(\vec{A}) = 0.17$, were obtained by using the pre-exponential factors included in the SD mechanism (with revised $k(T)$ for the reaction $CH_3 + OH \leftrightarrow CH_2^* + H_2O$, see Appendix B as the initial conditions for the optimization. For each reaction i, the optimized pre-exponential factor, $A_{i,\text{opt}}$, is the product of the original value, A_i, with the corresponding multiplier ($A_{i,\text{opt}} = A_i \cdot f_{i,\text{orig}}$). To obtain the $f_{i,\text{inv}}$ multipliers (see Table 4), a second adjustment procedure was performed taking as initial conditions the pre-exponential factors of the original SD mechanism divided by $f_{i,\text{orig}}$, i.e., $A_i/f_{i,\text{orig}}$, or the lower/upper bounds of optimization if the ratio $A_i/f_{i,\text{orig}}$ falls out-of-bounds. This second adjustment, starting in a remote location of the optimization space, was performed to check for the existence of other local minima of $F(\vec{A})$.

Figure 3 compares numerical values of S_{LIF}/S_R and δ_{CH}, obtained with the un-modified SD mechanism and the two optimized models corresponding to $f_{i,\text{orig}}$ and $f_{i,\text{inv}}$, against the experiments reported in [3]. The error bars applied on the experimental data represent the 95% interval of confidence for the variability in the measurements (precision). As per the comparative diagnostic approach discussed above [20], the accuracy of the measurements, e.g., the uncertainty in the CH-LIF model, is reported on the numerical values. This information is omitted
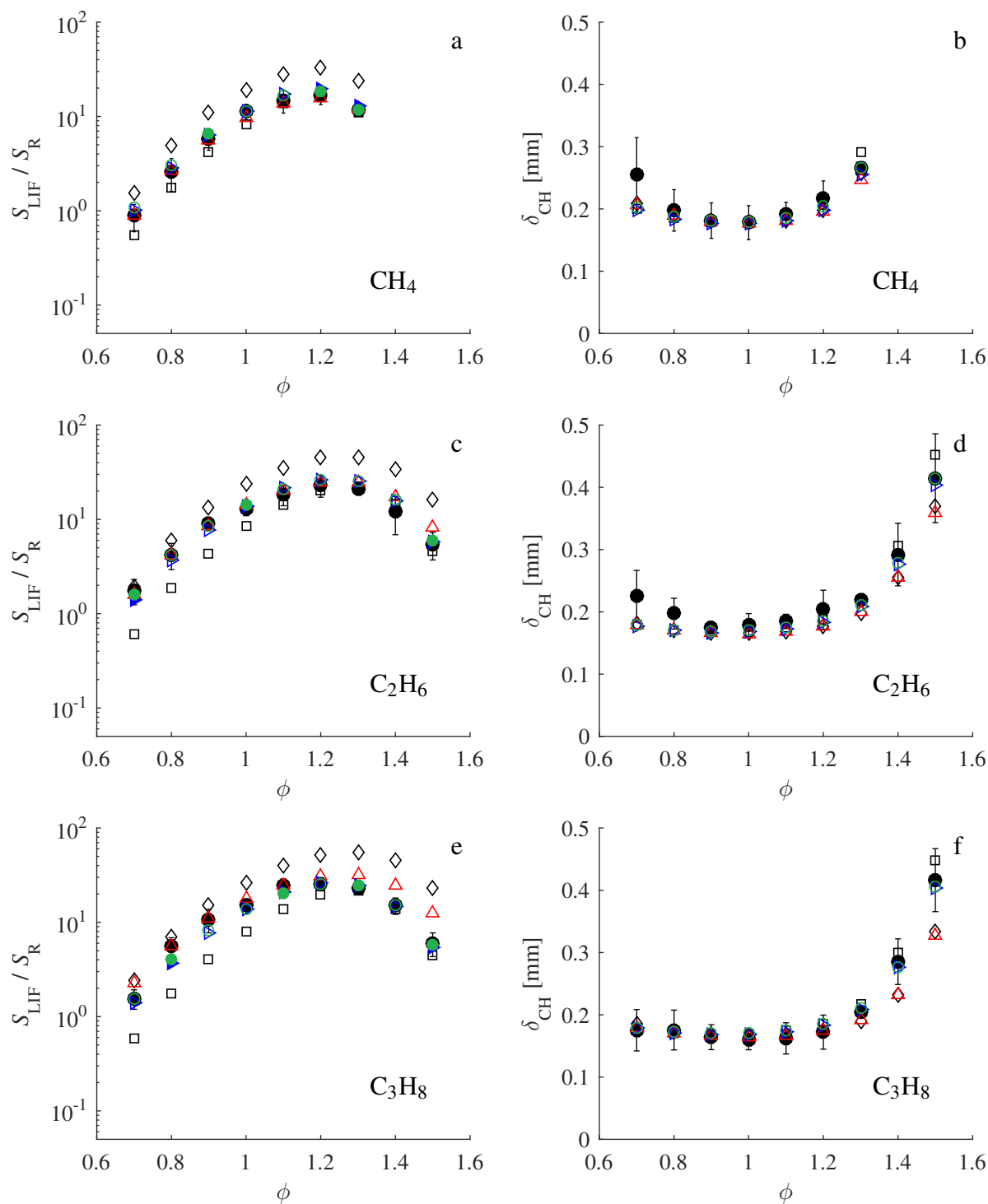
---

[1]For the reaction $CH_3 + OH \leftrightarrow CH_2^* + H_2O$, the multiplier values apply to the updated specific rate description $k(T) = 1.57 \cdot 10^{17} \cdot T^{-1.225} \cdot \exp\left(-1811/R_u \cdot T\right)$ cm³/mol−s, not to the nominal specific rate included in the SD mechanism. See Appendix B.

Fig. 3.   Measured [3] and simulated values of S_{LIF}/S_R and δ_{CH} for methane, ethane, and propane premixed flames. Legend: ● experiments, □ SD (un-modified), ○ $f_{i,\text{orig}}$ (Table 3), ▷ $f_{i,\text{inv}}$ (Table 4), ◇ GRI (un-modified), and △ GRI with the rate coefficients of Table 3. The solid blue and green symbols correspond to data points included in the optimization and adjusted against the experimental targets presented in Table 2. Note the logarithmic scale on plots a, c, and e.

here for the sake of brevity and clarity of the figures. However, it was verified that all values of S_{LIF}/S_R predicted by the optimized models are within the limits of uncertainty considering

the accuracy and precision of the measurements. Hence, even if the set of $f_{i,\text{inv}}$ multipliers presents a slightly higher value of $F(\vec{A})$ (see Table 4), both mechanisms are equally valid based

Table 3. Rate coefficients corresponding to the $f_{i,\mathrm{orig}}$ set of multipliers, which yield $F(\vec{A}) = 0.17$.

Reactions	$f_{i,\mathrm{orig}}$	$A_{i,\mathrm{opt}}$ [cm, mol, s]	n_i	$E_{a,i}$ [cal, mol]
$CH + O_2 \leftrightarrow HCO + O$	**0.4747**	$8.403 \cdot 10^{10}$	0.760	−478.01
$CH_2 + OH \leftrightarrow CH + H_2O$	0.8519	$9.626 \cdot 10^{6}$	2.000	2999.52
$CH_2 + H \leftrightarrow CH + H_2$	3.198	$1.925 \cdot 10^{13}$	0.000	−1787.76
$H + CH_3 (+M) \leftrightarrow CH_4 (+M)$				
High-pressure limit	0.7847	$9.965 \cdot 10^{15}$	−0.630	383.00
Low-pressure limit		$1.938 \cdot 10^{33}$	−4.760	2440.00
$CH_3 + OH \leftrightarrow CH_2^* + H_2O$	1.502	$2.357 \cdot 10^{17}$	−1.225	1811.00
$CH + H_2O \leftrightarrow CH_2O + H$	**3.549**	$4.152 \cdot 10^{15}$	−0.750	0.00
$CH_2 + O_2 \leftrightarrow CO + OH + H$	**0.8482**	$5.581 \cdot 10^{12}$	0.000	1491.40
$\leftrightarrow CO_2 + H_2$		$2.231 \cdot 10^{12}$	0.000	1491.40
$CH_2CO + O \leftrightarrow CH_2 + CO_2$	**1.502**	$3.003 \cdot 10^{13}$	0.000	2294.46

Table 4. Rate coefficients corresponding to the $f_{i,\mathrm{inv}}$ set of multipliers, which yield $F(\vec{A}) = 0.25$.

Reactions	$f_{i,\mathrm{inv}}$	$A_{i,\mathrm{opt}}$ [cm, mol, s]	n_i	$E_{a,i}$ [cal, mol]
$CH + O_2 \leftrightarrow HCO + O$	**0.4747**	$8.403 \cdot 10^{10}$	0.760	−478.01
$CH_2 + OH \leftrightarrow CH + H_2O$	**2.102**	$2.375 \cdot 10^{7}$	2.000	2999.52
$CH_2 + H \leftrightarrow CH + H_2$	0.7596	$4.573 \cdot 10^{12}$	0.000	−1787.76
$H + CH_3 (+M) \leftrightarrow CH_4 (+M)$				
High-pressure limit	0.5453	$6.926 \cdot 10^{15}$	−0.630	383.00
Low-pressure limit		$1.347 \cdot 10^{33}$	−4.760	2440.00
$CH_3 + OH \leftrightarrow CH_2^* + H_2O$	0.8936	$1.403 \cdot 10^{17}$	−1.225	1811.00
$CH + H_2O \leftrightarrow CH_2O + H$	**2.281**	$2.669 \cdot 10^{15}$	−0.750	0.00
$CH_2 + O_2 \leftrightarrow CO + OH + H$	**0.8482**	$5.581 \cdot 10^{12}$	0.000	1491.40
$\leftrightarrow CO_2 + H_2$		$2.231 \cdot 10^{12}$	0.000	1491.40
$CH_2CO + O \leftrightarrow CH_2 + CO_2$	**1.490**	$2.981 \cdot 10^{13}$	0.000	2294.46

on the comparison with experimental $S_{\mathrm{LIF}}/S_{\mathrm{R}}$ data. Also, the values of δ_{CH} reported in Fig.3 represent the full width at half-maximum (FWHM) of the one-dimensional (1D) CH-LIF profiles, which corresponds to the width of the 1D CH concentration profiles magnified by the imaging-system blur, accounted for through convolution of a Gaussian point-spread function [3].

For all fuels, the optimization significantly improves the agreement of the numerical LIF signals with the experiments, namely by correcting the overpredicted decline in $S_{\mathrm{LIF}}/S_{\mathrm{R}}$ as the stoichiometry is shifted to leaner mixtures starting from $\phi = 1.2$. The reactions improving the stoichiometric dependence of CH formation have their multiplier shown in boldface in Tables 3 and 4. They are reactions with a decreasing (increasing) trend of L.S. $(X_{\mathrm{CH,peak}}, i)$ with ϕ (see Fig.1), and for which the specific rate is raised (reduced) during the adjustment, i.e., that have a multiplier value > 1 (< 1). The larger are the L.S. $(X_{\mathrm{CH,peak}}, i)$ and the relative change in the specific rate, the larger is the impact on the model response. The main contributors are the reactions $CH + O_2 \leftrightarrow HCO + O$ and $CH + H_2O \leftrightarrow CH_2O + H$, as well as $CH_2 + OH \leftrightarrow CH + H_2O$ for the model with the $f_{i,\mathrm{inv}}$ multipliers. These reactions are directly involved in the formation and consumption of methylidyne. It must be remembered that the specific rate of the reaction $CH_3 + OH \leftrightarrow CH_2^* + H_2O$ was updated prior to the optimization process (see Fig.10 and related discussion). In this context, changing $k(T)$ from the nominal definition in the SD mechanism to the optimized rate is expected not to significantly improve ($f_{i,\mathrm{orig}}$), or to worsen ($f_{i,\mathrm{inv}}$), the trend of $[\mathrm{CH}]_{\mathrm{peak}}$ vs. ϕ. The other, non-boldface, reactions in Tables 3 and 4 mostly impact CH predictions for rich flames, e.g., $H + CH_3 (+M) \leftrightarrow CH_4 (+M)$, or compensate for the change in the specific rate of the other reactions to achieve the proper amplitude (absolute values) of $[\mathrm{CH}]_{\mathrm{peak}}$.

Interestingly, the agreement in terms of δ_{CH} for rich, $\phi \geq 1.3$, flames is also enhanced, even if the thickness of the CH layer was not considered as an optimization target. From flame theory, the reaction zone thickness is proportional to α/s_{L}, where α is the thermal diffusivity, and S_{L} is the laminar flame speed. Among the reactions included in the optimization, the laminar flame speed is principally sensitive to the rate of the reaction $H + CH_3 (+M) \leftrightarrow CH_4 (+M)$, particularly for rich mixtures [5,7]. Decreasing the specific rate of this reaction as prescribed by the two optimized mechanisms leads to an increase in the burning rate of rich flames which, based on flame theory, should make the flame, and consequently the CH layer, thinner thus improving the accuracy of the predicted δ_{CH} values. For lean methane and ethane flames, the discrepancies between the numerical and experimental values of δ_{CH} were attributed to weak signal-to-noise ratios at these conditions artificially broadening the experimental CH layer thickness [3]. For all other fuels and equivalence ratios, the values of δ_{CH} predicted by the optimized mechanisms are consistent with the already accurate estimations of the SD model.

To determine if the specific rates derived in the current work apply to other thermochemical mechanisms, additional simulations were performed with the GRI model. As shown in Fig.3, the original GRI mechanism generally over-predicts the experiments beyond uncertainty and, for ethane and propane flames, the disagreement grows with the equivalence ratio. Inserting the optimized rate coefficients of Table 3 in the GRI mechanism results in CH-LIF signals and δ_{CH} values agreeing, within uncertainty, with the experimental data for methane, ethane, and propane ($\phi \leq 1.2$) flames. Consequently, the sets of optimized specific rates presented in this study are not restricted to the San Diego model. They can be used in other kinetic mechanisms, which should be benchmarked against the experimental data provided in [3].

The two sets of optimized specific rates are superimposed as green long-dashed ($f_{i,\mathrm{orig}}$), and blue dash-dotted ($f_{i,\mathrm{inv}}$) curves in Figs. 6 to 13 in Appendix B. It is difficult, as all mechanisms have their own set of elementary reactions, to identify a

single cause for the generalized problem of over-predicted decline in [CH]$_{peak}$ as ϕ decreases, and to suggest a single solution to make all kinetic models accurate. Nevertheless, a few observations can be made based on the current optimization:

- both optimized mechanisms have a multiplier of 0.4747 for the reaction $CH + O_2 \leftrightarrow HCO + O$, which yields a $k(T)$ description lower than all considered mechanisms in Fig.6, and in line with the low temperature recommendation of Baulch et al. [22]. The specific rate of this reaction is likely overestimated in most thermochemical mechanisms and, since L.S. $\left(X_{CH,peak}, i\right)$ increases with ϕ for this reaction, reducing its specific rate would improve the stoichiometric dependence of [CH]$_{peak}$ predictions.

- the improper stoichiometric dependence of [CH]$_{peak}$ is solved by adjusting the specific rate of a few key reactions identified in Figs. 1 and 2. Additional reactions do not need to be included in the mechanisms; the simple structure of the SD model is sufficient to accurately predict CH formation over a range of equivalence ratios.

- the existence of two sets of optimized multipliers, which yield CH-LIF signal predictions agreeing, within uncertainty, with the experimental data, demonstrates the need for 1) further experimental and/or numerical fundamental studies to reduce the uncertainty in the specific rate of the reactions (see Appendix B), and/or 2) additional, independent experimental targets, to constrain the optimization and decide on a single set of rate coefficients.

- as shown in Fig.7, $k(T)$ for the $f_{i,orig}$ set of multipliers is in fair agreement with the widely used rate description for the reaction $CH_2 + OH \leftrightarrow CH + H_2O$, while the specific rate of the mechanism with $f_{i,inv}$ lies close to the upper optimization bound. Furthermore, the former is fairly consistent with the rates included in the NUIG2 and KON mechanisms for the reaction $CH_2 + H \leftrightarrow CH + H_2$, while the latter sits on the lower bound of optimization, below the specific rate descriptions of all mechanisms (see Fig.8). Based on these arguments, one could favor the $f_{i,orig}$ set of multipliers.

- both optimizations maintain a specific rate description approximately an order of magnitude higher than the mechanisms [5–8] and the recommendation of Baulch et al. [22] for the reaction $CH_2CO + O \leftrightarrow CH_2 + CO_2$. Based on Fig.1, increasing the specific rate of this reaction contributes to solve the problem with the stoichiometric dependence of [CH]$_{peak}$, which aggravates for alkane chain-lengths longer than C$_1$ [3].

4 Conclusion

This paper presented an optimization of the San Diego combustion mechanism [4] against the experimentally-determined CH concentration and layer thickness data presented in [3]. Nine elementary reactions were selected, which featured a large uncertainty in their specific rate and a significant impact on the formation of methylidyne. These reactions, interacting with

the CH formation route, require further consideration from the combustion community to converge toward a unique, accurate description of their specific rate. The optimization was constrained by meticulously selected bounds on the value of the pre-exponential factors, and performed using a non-linear, quasi-Newton, multi-variate algorithm minimizing an objective function defined as the sum of squares of the relative difference between numerical CH-LIF signals and a selection of experimental data points. The adjustment procedure provided two mechanisms that agree, within uncertainty, with the experimentally-determined CH-LIF layer thicknesses and signal intensities presented in [3].

The over-predicted decrease in CH formation as stoichiometry is shifted to lean mixtures observed in [3,14,15] is resolved, primarily by adjusting the rate of the reactions $CH + O_2 \leftrightarrow HCO + O$, $CH_2 + OH \leftrightarrow CH + H_2O$, and $CH + H_2O \leftrightarrow CH_2O + H$, and does not require the addition of supplementary reactions to the simple structure of the San Diego mechanism. The results suggest that the rate of the reaction $CH + O_2 \leftrightarrow HCO + O$ should be reduced, and that of the reaction $CH_2CO + O \leftrightarrow CH_2 + CO_2$ increased, in most thermochemical mechanisms.

The optimized specific rates provided in this study are not exclusive to the San Diego mechanism. They were successfully implemented in the GRI Mech 3.0 model to improve its predictive performance in terms of CH concentrations.

5 Permission for Use

Acknowledgements

References

[1] Watson, G., Versailles, P., and Bergthorson, J., 2017. "NO formation in rich premixed flames of C$_1$-C$_4$ alkanes and alcohols". *Proc. Combust. Inst.,* **36**, pp. 627–635.

[2] Watson, G. M. G., Versailles, P., and Bergthorson, J. M., 2016. "NO Formation in premixed flames of C$_1$-C$_3$ alkanes and alcohols". *Combust. Flame,* **169**, pp. 242–260.

[3] Versailles, P., Watson, G. M. G., Lipardi, A. C. A., and Bergthorson, J. M., 2016. "Quantitative CH measurements in atmospheric-pressure , premixed flames of C$_1$-C$_4$ alkanes". *Combust. Flame,* **165**, pp. 109–124.

[4] University of California at San Diego, 2005. "Chemical-Kinetic Mechanisms for Combustion Applications", San Diego Mechanism web page, Mechanical and

Aerospace Engineering (Combustion Research). http://combustion.ucsd.edu.

[5] Smith, G. P., Golden, D. M., Frenklach, M., Moriarty, N. W., Eiteneer, B., Goldenberg, M., Bowman, C. T., Hanson, R. K., Song, S., Gardiner, W. C., Lissianski, V. V., and Qin, Z., 1999. GRI-Mech 3.0. http://www.me.berkeley.edu/gri_mech/.

[6] Wang, H., You, X., Joshi, A. V., Davis, S. G., Laskin, A., Egolfopoulos, F., and Law, C. K., 2007. USC Mech Version II. High-Temperature Combustion Reaction Model of $H_2/CO/C_1$-C_4 Compounds. http://ignis.usc.edu/USC_Mech_II.htm.

[7] Metcalfe, W. K., Burke, S. M., Ahmed, S. S., and Curran, H. J., 2013. "A Hierarchical and Comparative Kinetic Modeling Study of C_1-C_2 Hydrocarbon and Oxygenated Fuels". *Int. J. Chem. Kin.,* **45**(10), pp. 638–675.

[8] Zhou, C. W., Li, Y., O'Connor, E., Somers, K. P., Thion, S., Keesee, C., Mathieu, O., Petersen, E. L., DeVerter, T. A., Oehlschlaeger, M. A., Kukkadapu, G., Sung, C. J., Alrefae, M., Khaled, F., Farooq, A., Dirrenberger, P., Glaude, P. A., Battin-Leclerc, F., Santner, J., Ju, Y., Held, T., Haas, F. M., Dryer, F. L., and Curran, H. J., 2016. "A comprehensive experimental and modeling study of isobutene oxidation". *Combust. Flame,* **167**, pp. 353–379.

[9] Konnov, A. A., 2009. "Implementation of the NCN pathway of prompt-NO formation in the detailed reaction mechanism". *Combust. Flame,* **156**(11), pp. 2093–2105.

[10] Jacob, D. J., 2000. *Introduction to Atmospheric Chemistry*. Princeton University Press.

[11] Vallero, D., 2014. *Fundamentals of Air Pollution*, fifth ed. Academic Press.

[12] Lieuwen, T., and Yang, V., 2013. *Gas Turbine Emissions*. Cambridge Edition.

[13] Miller, J. A., and Bowman, C. T., 1989. "Mechanism and modeling of nitrogen chemistry in combustion". *Prog. Energy Combust. Sci.,* **15**, pp. 287–338.

[14] Sutton, J. A., and Driscoll, J. F., 2003. "Optimization of CH Fluorescence Diagnostics in Flames: Range of Applicability and Improvements with Hydrogen Addition". *Appl. Opt.,* **42**(15), pp. 2819–2828.

[15] Bergthorson, J. M., 2005. "Experiments and Modeling of Impinging Jets and Premixed Hydrocarbon Flames". PhD thesis, California Institute of Technology.

[16] Davis, S. G., Law, C. K., and Wang, H., 1999. "Propene pyrolysis and oxidation kinetics in a flow reactor and laminar flames". *Combust. Flame,* **119**, pp. 375–399.

[17] University of California at San Diego, 2003. "Chemical-Kinetic Mechanisms for Combustion Applications", San Diego Mechanism web page, Mechanical and Aerospace Engineering (Combustion Research). http://combustion.ucsd.edu.

[18] Frenklach, M., Wang, H., and Rabinowitz, M. J., 1992. "Optimization and analysis of large chemical kinetic mechanisms using the solution mapping method-combustion of methane". *Prog. Energy Combust. Sci.,* **18**, pp. 47–73.

[19] Gilbert, R. G., Luther, K., and Troe, J., 1983. "Theory of Thermal Unimolecular Reactions in the Fall-off Range. II Weak Collision Rate Constants". *Ber. Bunsenges. Phys. Chem.,* **87**, pp. 169–177.

[20] Connelly, B. C., Bennett, B. A. V., Smooke, M. D., and Long, M. B., 2009. "A paradigm shift in the interaction of experiments and computations in combustion research". *Proc. Combust. Inst.,* **32**(1), pp. 879–886.

[21] Reaction Design, 2013. Chemkin-Pro Release 15131.

[22] Baulch, D. L., Bowman, C. T., Cobos, C. J., Cox, R. A., Just, T., Kerr, J. A., Pilling, M. J., Stocker, D., Troe, J., Tsang, W., Walker, R. W., and Warnatz, J., 2005. "Evaluated Kinetic Data for Combustion Modeling: Supplement II". *J Phys. Chem Ref. Data,* **34**(3), pp. 757–1397.

[23] Baulch, D. L., Cobos, C. J., Cox, R. A., Esser, C., Frank, P., Just, T., Kerr, J. A., Pilling, M. J., Troe, J., Walker, R. W., and Warnatz, J., 1992. "Evaluated Kinetic Data for Combustion Modelling". *J. Phys. Chem. Ref. Data,* **21**(3), p. 411.

[24] Tsang, W., and Hampson, R. F., 1986. "Chemical Kinetic Data Base for Combustion Chemistry. Part I. Methane and Related Compounds". *J. Phys. Chem. Ref. Data,* **15**(3), pp. 1087–1279.

[25] Versailles, P., 2017. "CH formation in premixed flames of C_1–C_4 alkanes: assessment of current chemical modelling capability against experiments". PhD thesis, McGill University.

[26] Goodwin, D. G., Moffat, H. K., and Speth, R. L., 2016. Cantera: An object-oriented software toolkit for chemical kinetics, thermodynamics, and transport processes. Version 2.2.1, http://www.cantera.org.

[27] Turányi, T., Zalotai, L., Dóbé, S., and Bérces, T., 2002. "Effect of the uncertainty of kinetic and thermodynamic data on methane flame simulation results". *Phys. Chem. Chem. Phys.,* **4**(12), pp. 2568–2578.

[28] Argonne National Laboratory. "Active Thermochemical Tables, version 1.118". http://atct.anl.gov/.

[29] Fomin, A., Zavlev, T., Alekseev, V. A., Rahinov, I., Cheskis, S., and Konnov, A. A., 2016. "Experimental and modelling study of $^1CH_2$ in premixed very rich methane flames". *Combust. Flame,* **171**, pp. 198–210.

[30] Glarborg, P., Miller, J. A., and Kee, R. J., 1986. "Kinetic modeling and sensitivity analysis of nitrogen oxide formation in well-stirred reactors". *Combust. Flame,* **65**, pp. 177–202.

[31] CRECK Modeling Group, 2014. Creck kinetics model (version 1412). http://creckmodeling.chem.polimi.it/index.php/menu-kinetics/menu-kinetics-detailed-mechanisms.

[32] Gokulakrishnan, P., Fuller, C. C., Klassen, M. S., Joklik, R. G., Kochar, Y. N., Vaden, S. N., Lieuwen, T. C., and Seitzman, J. M., 2014. "Experiments and modeling of propane combustion with vitiation". *Combust. Flame,* **161**(8), pp. 2038–2053.

[33] Leung, K. M., and Lindstedt, R. P., 1995. "Detailed Ki-

netic Modeling of C_1-C_3 Alkane Diffusion Flames". *Combust. Flame,* **102**(94), pp. 129–160.

[34] Baulch, D. L., Cobos, C. J., Cox, R. A., Frank, P., Hayman, G., Just, T., Kerr, J. A., Murrells, T., Pilling, M. J., Troe, J., Walker, R. W., and Warnatz, J., 1994. "Evaluated Kinetic Data for Combustion Modeling. Supplement I". *J. Phys. Chem. Ref. Data,* **23**(6), pp. 847–848.

[35] Jasper, A. W., Klippenstein, S. J., Harding, L. B., and Ruscic, B., 2007. "Kinetics of the reaction of methyl radical with hydroxyl radical and methanol decomposition". *J. Phys. Chem. A,* **111**(10), pp. 3932–3950.

[36] Dombrowsky, C., and Wagner, H. G., 1992. "Investigation of the $^3CH_2 + O_2$ reaction in shock waves". *Ber. Bunsenges. Phys. Chem.,* **96**(8), pp. 1048–1055.

[37] Lee, P. F., Matsui, H., Chen, W. Y., and Wang, N. S., 2012. "Production of H and O $\left(^3P\right)$ atoms in the reaction of CH_2 with O_2". *J. Phys. Chem. A,* **116**(37), pp. 9245–9254.

[38] Böhland, T., Temps, F., and Wagner, H. G., 1984. "Direct determination of the rate constant for the reaction $CH_2 + O_2$ with a lmr-spectrometer". *Ber. Bunsenges. Phys. Chem.,* **88**(5), pp. 455–458.

[39] Darwin, D. C., Young, A. T., Johnston, H. S., and Moore, C. B., 1989. "Rate constants for CH_2 $(\tilde{X}^3B_1)$ removal by O_2, NO and C_2H_2 from infrared diode laser flash kinetic spectroscopy". *J. Phys. Chem.,* **93**(3), pp. 1074–1078.

[40] Vinckier, C., and Debruyn, W., 1979. "Temperature dependence of the reactions of methylene with oxygen atoms, oxygen, and nitric oxide". *J. Phys. Chem.,* **83**(16), pp. 2057–2062.

[41] Dombrowsky, C., Hwang, S. M., Röhrig, M., and Wagner, H. G., 1992. "The formation of O and H atoms in the reaction of CH_2 with O_2 at high temperatures". *Ber. Bunsenges. Phys. Chem.,* **96**(2), pp. 194–198.

[42] Hidaka, Y., Kimura, K., Hattori, K., and Okuno, T., 1996. "Shock tube and modeling study of ketene oxidation". *Combust. Flame,* **106**(1-2), pp. 155–167.

Appendix A: Effect of the uncertainties in the thermodynamic properties on the $[CH]_{peak}$ predictions

Inaccuracies in the thermodynamic properties can induce errors in the local temperature and, as a consequence, significantly impact the computed specific rates. Furthermore, in most thermochemical mechanisms, the specific rate of the reactions is only specified in the forward direction, and the backward specific rate obtained from the equilibrium constant computed from the entropy and heat of formation $(\Delta_f H_k^\circ)$ data, the latter generally bearing the largest uncertainty of all thermodynamic properties [27]. Therefore, in addition to the rate coefficients, the uncertainties in the thermodynamic parameters have the potential to induce errors in the CH concentration predictions.

To assess if thermodynamic properties should be included in the optimization, an analysis similar to that presented in Figs. 1 and 2 is performed. Figure 4 presents the logarithmic sensitivity of the maximum CH concentration to changes in the heat of formation of the individual species, L.S. $\left(X_{CH,peak}, k\right)$,
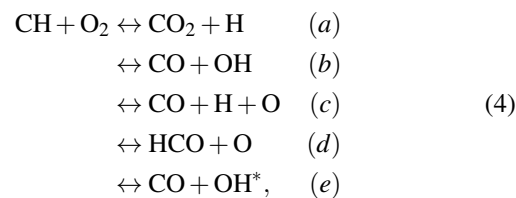
extracted from jet-wall stagnation flame simulations performed with Chemkin-Pro [21]. It is observed that L.S. $\left(X_{CH,peak}, k\right)$ can be as much as an order of magnitude larger than the logarithmic sensitivity of $[CH]_{peak}$ to variations in the specific rates (see Fig.2). However, the values of $\Delta_f H_k^\circ$ are known to a greater level of accuracy than specific rates. Figure 5 presents the products of L.S. $\left(X_{CH,peak}, k\right)$ with the relative uncertainty in the heat of formation of each species obtained from [28]. These values are as much as three orders of magnitude lower than the products of the logarithmic sensitivity with the relative uncertainty in the specific rates presented in Fig.2. Therefore, the error induced in $[CH]_{peak}$ by the uncertain thermodynamic parameters is negligible in comparison to the contribution of the rate coefficients. Consequently, only the pre-exponential factors of key reactions involved in the CH formation route are optimized in this study.

Appendix B: Bounds on the value of the active parameters

The bounds for the active parameters provided in Table 1 are determined by comparing the rate coefficients included in the SD mechanism to values available in the literature. The lower part of Figs. 6 to 13 presents, for each reaction included in the optimization, the specific rate descriptions from various sources. This review does not intend to be comprehensive, but rather to provide a reasonable range of adjustment for the active parameters. Net reaction rates normalized to unity, q_{net}, extracted from freely-propagating, premixed, CH_4-air flame simulations performed with the SD mechanism and solved with Chemkin-Pro [21] at three equivalence ratios ($\phi = 0.7$, 1.0, and 1.3), are shown in the upper part of these same figures to indicate the range of temperatures over which the reactions proceed.

Reaction $CH + O_2 \leftrightarrow HCO + O$

Oxidation of CH by O_2 is, along with the reaction $CH + H_2O \leftrightarrow CH_2O + H$, the principal sink of methylidyne included in thermochemical mechanisms. Baulch et al. [22] report 5 product channels for this reaction:

$$
\begin{aligned}
CH + O_2 &\leftrightarrow CO_2 + H &(a)\\
&\leftrightarrow CO + OH &(b)\\
&\leftrightarrow CO + H + O &(c)\\
&\leftrightarrow HCO + O &(d)\\
&\leftrightarrow CO + OH^*, &(e)
\end{aligned} \qquad (4)
$$

the last path expected to be of negligible importance. The mechanisms generally include a subset of these product channels; the SD, USC and GRI models feature channel (d) only, NUIG1 and NUIG2 (d) and (e), KON (b) and (d), and [29] (a)–(d). The overall, forward rate of reaction (4) can be written as:

$$
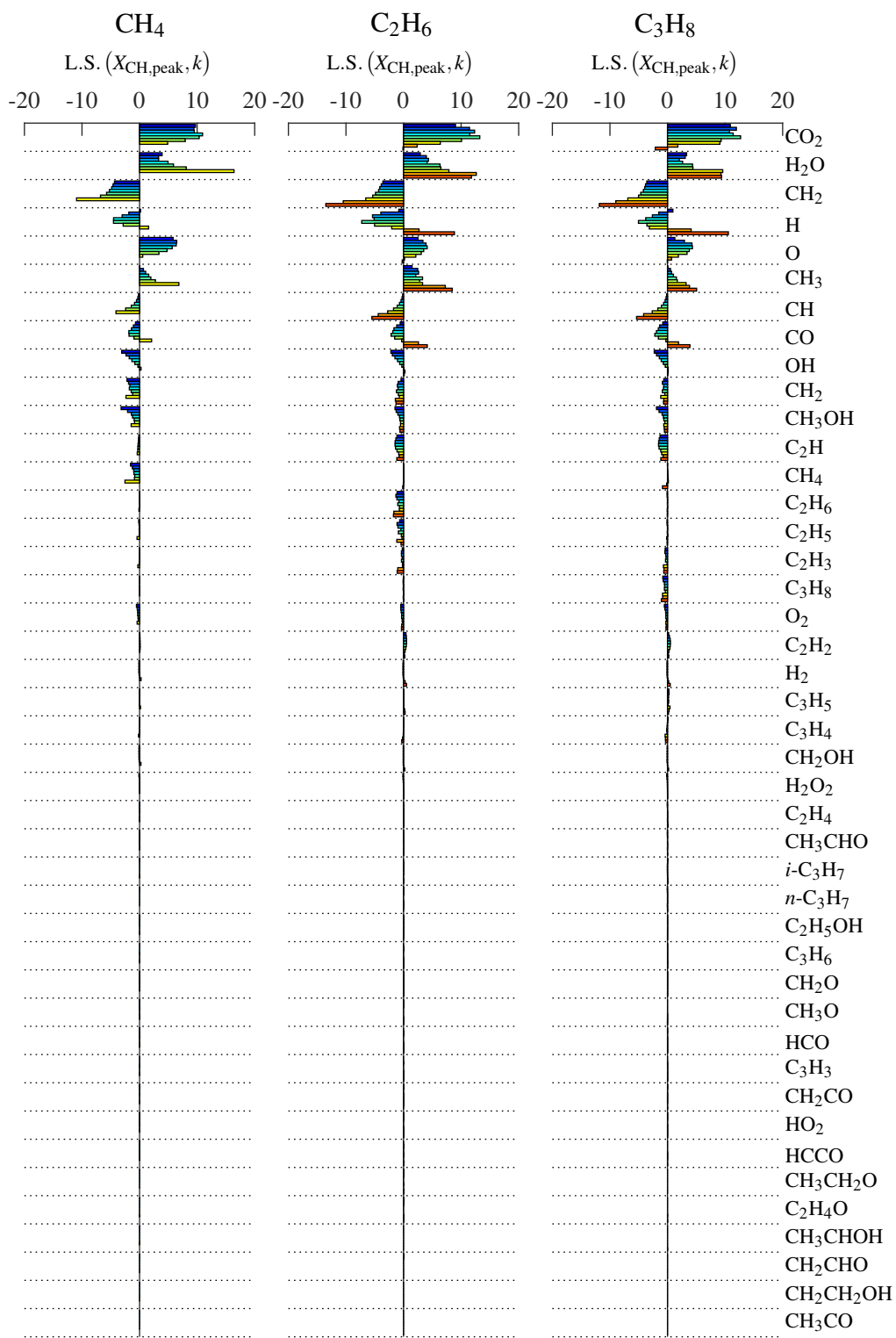\sum_i [CH][O_2] k_i = [CH][O_2] \sum_i k_i = [CH][O_2] k_{overall}. \quad (5)
$$

Fig. 4. Logarithmic sensitivity of the maximum CH mole fraction to the heat of formation of individual species, L.S. $(X_{CH,peak}, k)$. The species are sorted in decreasing order of $\sum\limits_{C_m H_n, \phi}$ L.S. $(X_{CH,peak}, k)^2$.

Figure 6 reports the overall specific rate ($k_{overall} = \sum_i k_i$) from various mechanisms, as well as the specific rates recommended by Baulch et al. [22] at low (290-800 K) and high (2200-3500 K) temperatures. $f_{i,high} = 2.456$ (upper, solid red curve in
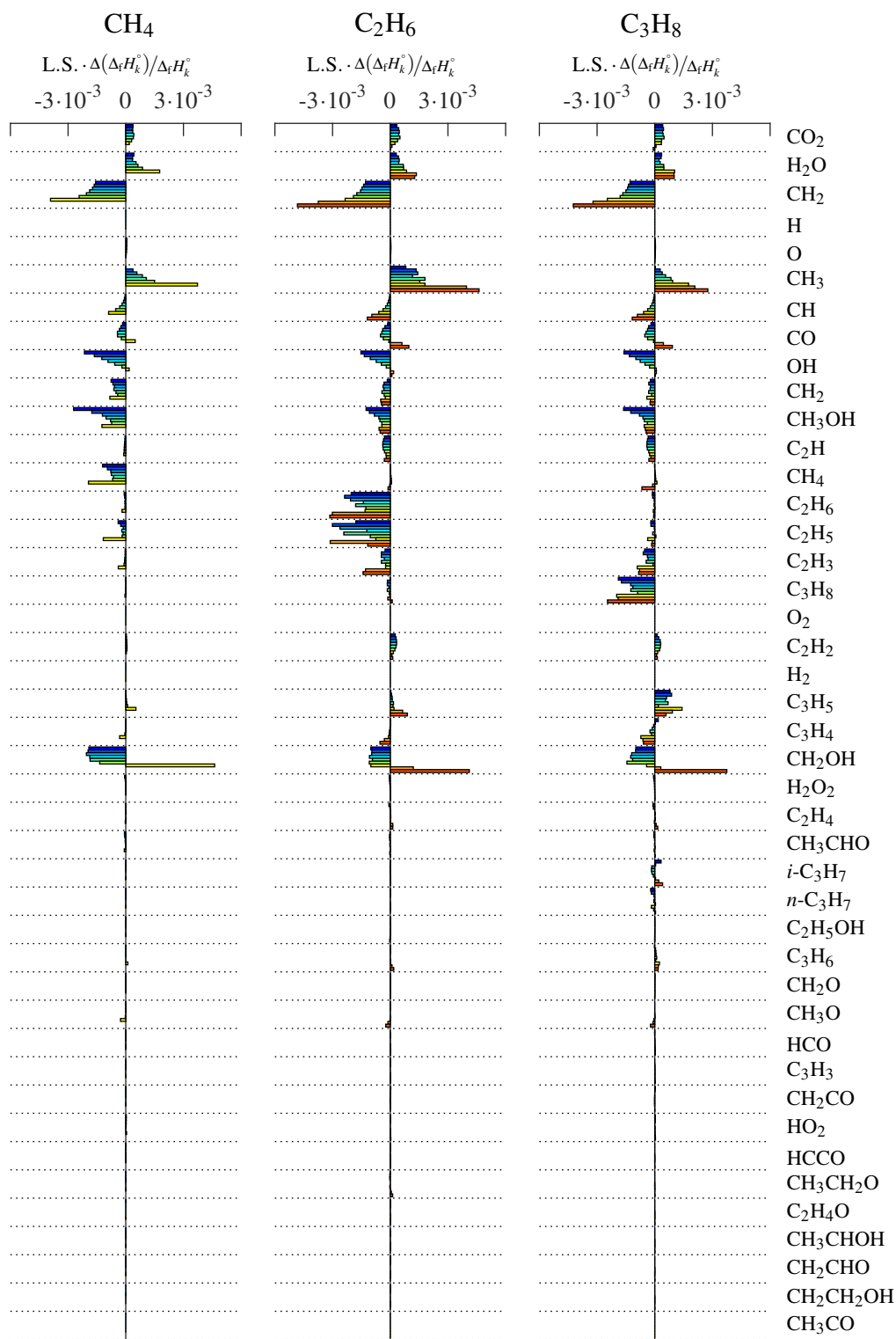
Fig. 5. Product of L.S. $\left(X_{\mathrm{CH,peak}}, k\right)$ with $\Delta\left(\Delta_f H_k^\circ\right)/\Delta_f H_k^\circ$. The relative errors are obtained from [28].

Fig.6) is adjusted to the upper uncertainty limit of the overall specific rate specified in [22] at 2200 K. Essentially, this implies that the SD mechanism is optimized such that all product channels identified in reaction (4) are lumped in the reaction $\mathrm{CH} + \mathrm{O}_2 \leftrightarrow \mathrm{HCO} + \mathrm{O}$. $1/f_{i,\mathrm{low}} = 0.4747$ is set such that the specific rate at 2250 K coincides with the USC mechanism. Adjusting $f_{i,\mathrm{low}}$ to the lower uncertainty limit at 800 K specified in [22] (lowest of the red-dotted lines in Fig.6) would al-
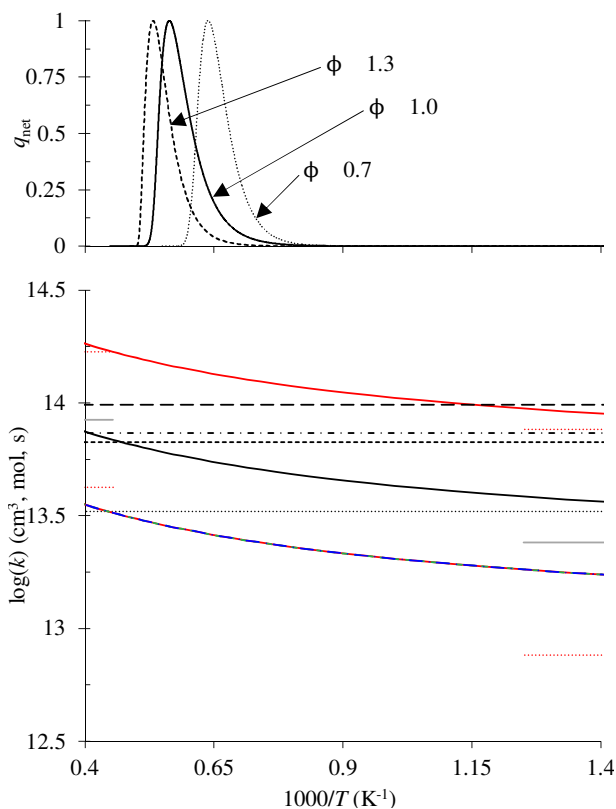
Fig. 6. q_{net} (top) and k (bottom) of the reaction $CH + O_2 \leftrightarrow$ products. Legend: —— SD, ········ USC, - - - - GRI, - · - NUIG1, — — KON, —— Baulch et al. [22] with corresponding uncertainty estimates (k_i/f_i and $k_i \cdot f_i$) ········ , bounds on active parameters $f_{i,low}$ and $f_{i,high}$ —— , and optimized specific rates corresponding to — — $f_{i,orig}$ and - · - $f_{i,inv}$, see Tables 3 and 4, respectively.

low the optimization procedure to achieve $k(T)$ values significantly lower than those provided in the mechanisms and the high-temperature recommendation of Baulch et al. [22] over the temperature range where this reaction proceeds (from ≈ 1355 K for lean flames to ≈ 1975 K for rich flames).

Reaction $CH_2 + OH \leftrightarrow CH + H_2O$

As shown in Fig.7, the specific rate description of the reaction $CH_2 + OH \leftrightarrow CH + H_2O$, one of the two principal pathways forming methylidyne along with the reaction $CH_2 + H \leftrightarrow CH + H_2$, is identical for the SD, USC, GRI, NUIG1, and KON mechanisms. This definition of $k(T)$ is used in many other models [8, 31–33]. This consistency must not be interpreted as an absolute exactness in the rate description of the reaction, and translated into narrow bounds of optimization. It is rather the reflection of the common origin of $k(T)$; all these mechanisms use the rate coefficients of the GRI model, which were obtained from [13].

Surprisingly, considering its significant contribution in the formation of CH, the reaction $CH_2 + OH \leftrightarrow CH + H_2O$ is not reported in the kinetic data reviews of Baulch et al. [22–24, 34]. Because of this lack of independent data, $f_{i,low}$ and $f_{i,high}$ are de-
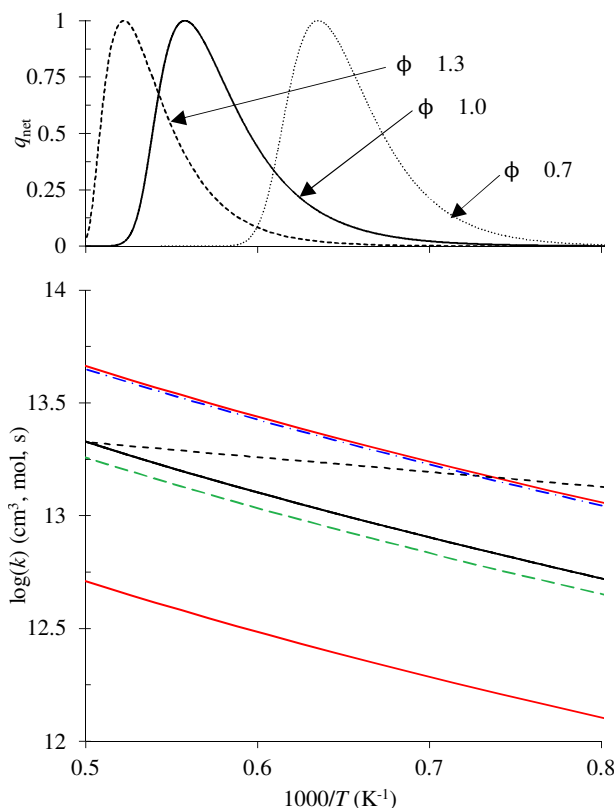
Fig. 7. q_{net} (top) and k (bottom) of the reaction $CH_2 + OH \leftrightarrow CH + H_2O$. Same legend as Fig.6, supplemented with - - - - [30].

termined by analogy with the reaction $CH_2 + OH \leftrightarrow CH_2O + H$, which has the same reactant species. For this reaction, the specific rates at the uncertainty limits evaluated by Tsang and Hampson [24] are 4.151 times lower and 2.168 times higher than the specific rate included in the SD mechanism. These multiplier values are selected to constrain the optimization of the rate of the reaction $CH_2 + OH \leftrightarrow CH + H_2O$ ($1/f_{i,low} = 0.2409$, and $f_{i,high} = 2.168$). As shown in Fig.7, these bounds surround the specific rate suggested in [30] for most of the temperature range over which the reaction occurs.

Reaction $CH_2 + H \leftrightarrow CH + H_2$

As shown in Fig.8, the mechanisms significantly disagree with regards to the rate of the reaction $CH_2 + H \leftrightarrow CH + H_2$. The specific rates included in the USC and GRI mechanisms are in fair agreement with the recommendation made by Baulch et al. in 2005 [22], while the SD and NUIG1 models best agree with the rate coefficients provided by the same group of authors in 1992 [23]. Including the rate descriptions of the KON and NUIG2 mechanisms does not point toward a preferred set of kinetic data, but rather suggests intermediate values of $k(T)$. The lower bound of optimization, $1/f_{i,low} = 0.7579$, is adjusted to the specific rate of the NUIG1 mechanism evaluated at 2000 K, and $f_{i,high} = 127.6$ corresponds to the upper error limit on $k(T = 2000K)$ provided in [22].

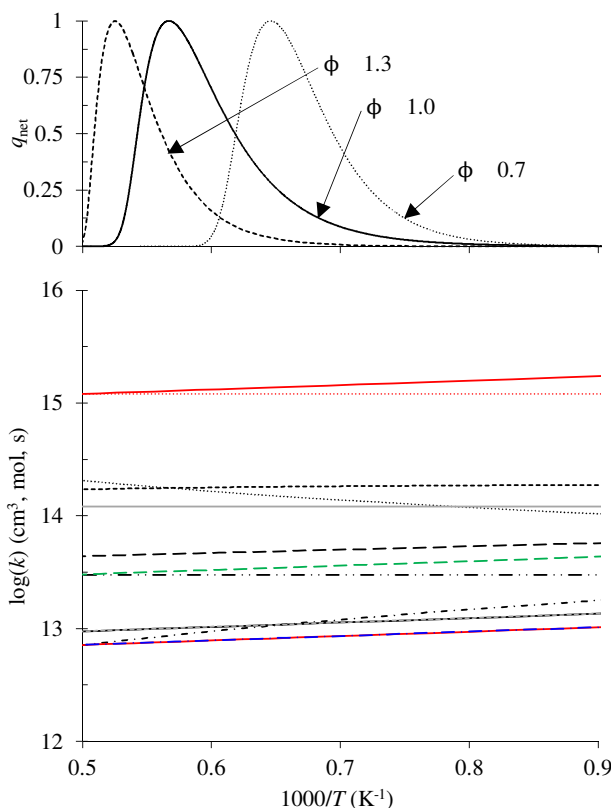Fig. 8. q_{net} (top) and k (bottom) of the reaction $CH_2 + H \leftrightarrow CH + H_2$. Same legend as Fig.6, supplemented with NUIG2 — · · — , and Baulch et al. (1992) [23] - - - - - .
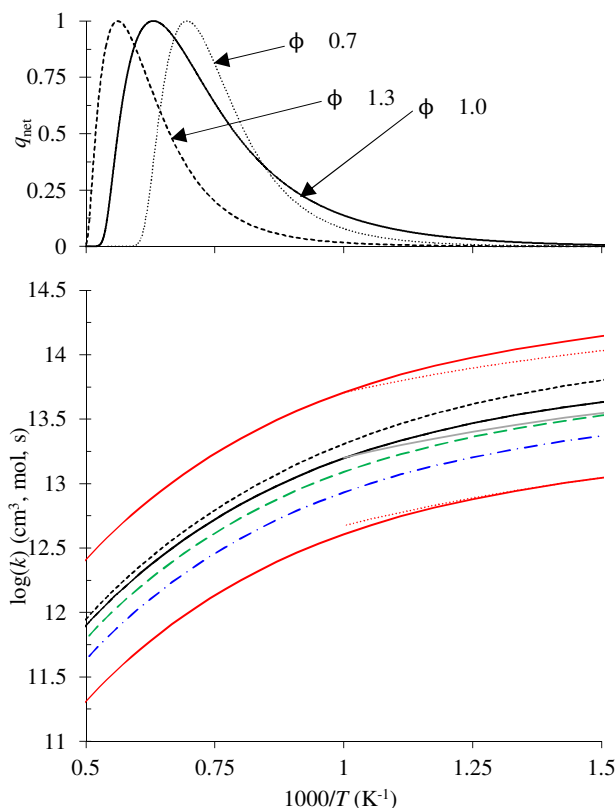

Fig. 9. q_{net} (top) and k (bottom) of the reaction $H + CH_3 (+M) \leftrightarrow CH_4 (+M)$. Same legend as Fig.6.

Reaction $H + CH_3 (+M) \leftrightarrow CH_4 (+M)$

As shown in Fig.9, the rate description of the three-body reaction $H + CH_3 (+M) \leftrightarrow CH_4 (+M)$ is fairly consistent among the SD, USC, GRI, and NUIG1 mechanisms, and with the recommended specific rate of [22] specified for temperatures up to 1000 K. The optimization bounds $1/f_{i,low} = 0.2577$ and $f_{i,high} = 3.246$ correspond to the lower and upper error limits of [22] at 667 K ($1000/T = 1.5$ K^{-1}) and 1000 K, respectively.

Reaction $CH_3 + OH \leftrightarrow CH_2^* + H_2O$

Figure 10 shows the significant disagreement among the mechanisms regarding the specific rate of the reaction $CH_3 + OH \leftrightarrow CH_2^* + H_2O$. The rate coefficients included in the NUIG1 mechanism (and NUIG2, which is not shown in the figure) are consistent with those determined theoretically by Jasper et al. [35]. Increasing values of the specific rate with decreasing temperatures are also noticed for the USC and GRI mechanisms, and the recommendation of Baulch et al. [22]. In contrast, the SD and KON models predict a rise in the specific rate with increasing temperatures. However, in its most recent release [29], the rate description of the KON mechanism was revised and the specific rate presents a temperature dependence similar to the other mechanisms [5–8], theoretical assessment [35], and review [22]. This advocates for an adjustment of the temperature dependence of the specific rate description included in the SD

model. For the optimization, the pre-exponential factor ($A = 1.57 \cdot 10^{17}$ cm^3/mol−s), temperature exponent ($n = -1.225$) and activation energy ($E_a = 1811$ cal·mol^{-1}) are adjusted such that $k(T)$ agrees with the recommendation of Baulch et al. [22] (note that only the original $k(T)$ of the SD model is shown in Fig.10, the new definition exactly overlaps [22]). The lower and upper bounds of optimization, $1/f_{i,low} = 0.3653$ and $f_{i,high} = 2.324$, match the specific rates of the NUIG1 mechanism at 2000 K and GRI model at 909 K ($1000/T = 1.1$ K^{-1}), respectively.

Reaction $CH + H_2O \leftrightarrow CH_2O + H$

As shown in Fig.11, there is a significant level of uncertainty in the rate coefficients of the reaction $CH + H_2O \leftrightarrow CH_2O + H$. Baulch et al. [22] provide a recommended specific rate for temperatures up to 1000 K, with an uncertainty factor $f = 10$. The rate description of the NUIG1 mechanism lies close to the upper error limit prescribed in [22], while the rate coefficients included in the SD, GRI and USC models yield lower values of $k(T)$. The lower bound of optimization, $1/f_{i,low} = 3.823 \cdot 10^{-2}$, is adjusted to the lower error limit included in [22] evaluated at $T = 1000$ K, while $f_{i,high} = 5.295$ corresponds to the specific rate at 2000 K of the NUIG1 mechanism.

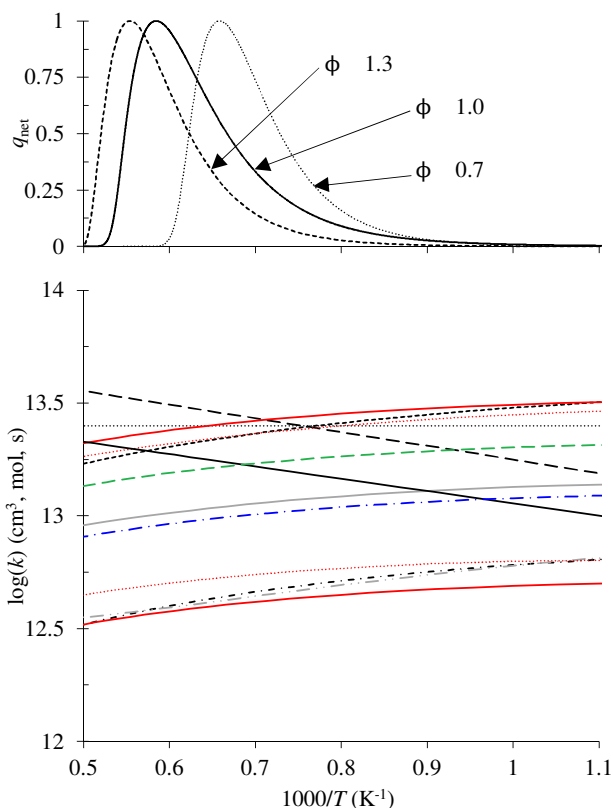Fig. 10. q_{net} (top) and k (bottom) of the reaction $CH_3 + OH \leftrightarrow CH_2^* + H_2O$. Same legend as Fig.6, supplemented with — · · — [35].
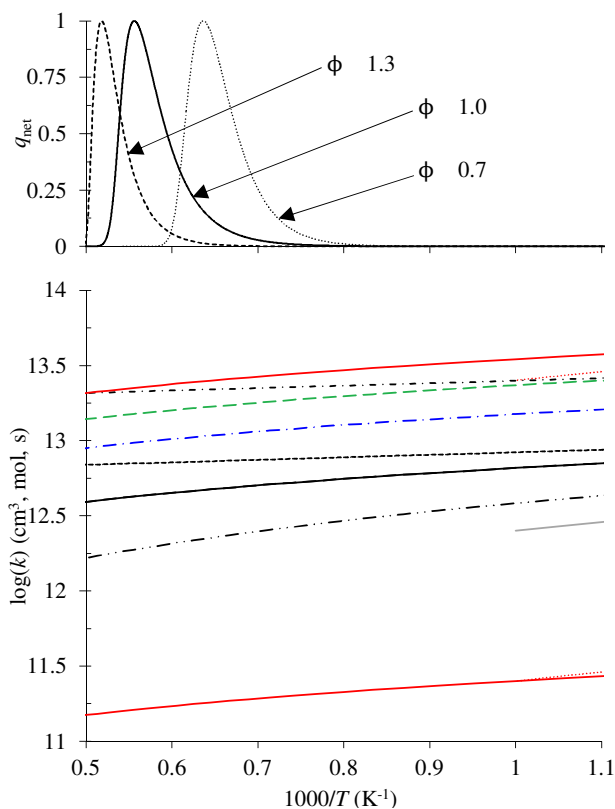
Fig. 11. q_{net} (top) and k (bottom) of the reaction $CH + H_2O \leftrightarrow CH_2O + H$. Same legend as Fig.8.

Reactions $CH_2 + O_2 \leftrightarrow CO + OH + H$ **and** $CH_2 + O_2 \leftrightarrow CO_2 + H_2$

The reaction of triplet methylene with molecular oxygen is expected to possess multiple product channels [22, 29]:

$$
\begin{aligned}
CH_2 + O_2 &\leftrightarrow CO_2 + H_2 & (a)\\
&\leftrightarrow CO + OH + H & (b)\\
&\leftrightarrow CO + H_2O & (c)\\
&\leftrightarrow HOCO + H & (d)\\
&\leftrightarrow CO_2 + 2H & (e)\\
&\leftrightarrow HCO + OH & (f)\\
&\leftrightarrow CO + H_2 + O & (g)\\
&\leftrightarrow CH_2O + O. & (h)
\end{aligned}
\qquad (6)
$$
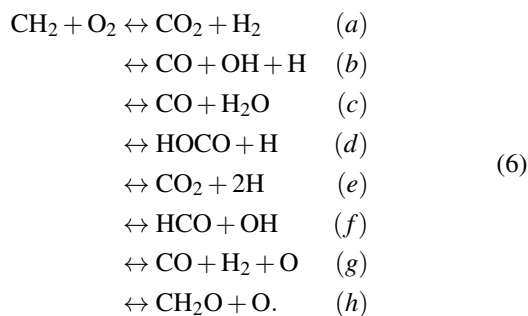
The exact branching among them remains uncertain [22, 36, 37], and the mechanisms generally include all, or a subset, of these reactions. Namely, the SD model considers channels (a) and (b).

Figure 12 presents the overall specific rate ($k_{overall} = \sum_i k_i$) of the reaction $CH_2 + O_2 \rightarrow$ products. Baulch et al., in 1992 [23] and 1994 [34], relying on specific rate measurements at room temperature [38, 39], and using the activation energy suggested by Vinckier and Debruyn [40] based on experiments performed over a temperature range of 295-600 K, recommended

$k(T) = 2.5 \cdot 10^{13} \exp(-750/T)$ cm^{3}mol^{-1}s^{-1} (short-dashed grey line in Fig.12), with an uncertainty factor $f = 10^{0.5} = 3.2$ at 1000 K. Many thermochemical mechanisms [4–8, 31] adopted the activation energy of ≈ 1500 cal·mol^{-1}, and adjusted the pre-exponential factor yielding specific rate descriptions within the uncertainty limits specified in [23, 34].

However, in 2005, Baulch et al. [22] included in their assessment an additional set of high temperature (1000-1750 K) experimental data [36, 41], which were approximately an order of magnitude below the specific rates predicted using the $k(T)$ description suggested in 1992 and 1994. They provided an updated, temperature-independent specific rate of $1.8 \cdot 10^{12}$ cm^{3}mol^{-1}s^{-1}, with an uncertainty factor $f = 10^{0.7} = 5.1$ at 1700 K.

Recently, experimental data [37] obtained at temperatures of 1850 to 2050 K contradicted the measurements of Dombrowsky et al. [36, 41], and were instead consistent with the extrapolation of the low-temperature data of Vinckier and Debruyn [40]. Lee et al. [37] proposed $k(T) = 1.65 \cdot 10^{13} \exp(-874/T)$ cm^{3}mol^{-1}s^{-1}, which falls within the uncertainty limits estimated by Baulch et al. in 1992 and 1994 [23, 34]. The specific rate description included in the KON mechanism was recently updated [29] (long-dashed grey line in Fig.12) to be consistent with Lee et al. [37]. For these reasons, the specific rates of the KON model and Baulch et al. (2005) [22] are excluded from the present analysis, and the
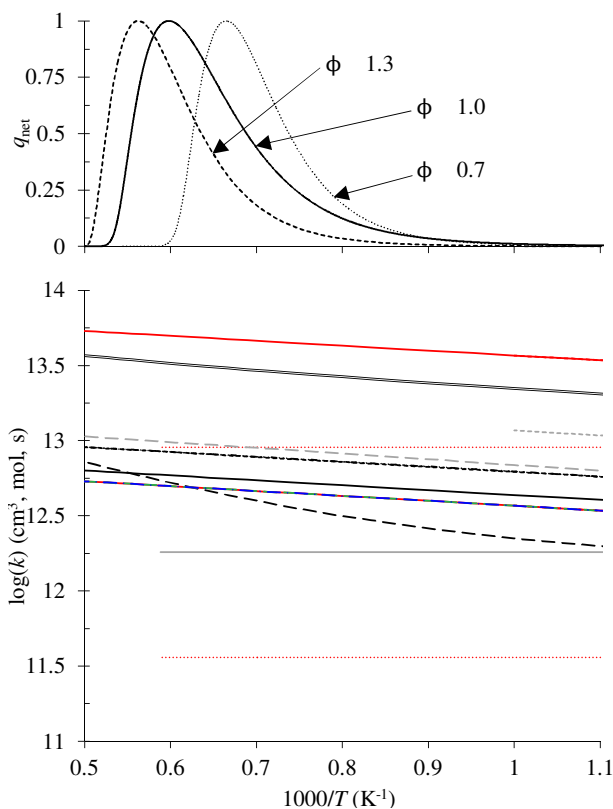

Fig. 12. Normalized net reaction rate of the reaction $CH_2 + O_2 \leftrightarrow CO + OH + H$ (top) and sum of the specific rates of reactions $CH_2 + O_2 \rightarrow$ products. Same legend as Fig.8, supplemented with data from the CRECK mechanism (version 1412) [31] ——— , and — — [29].

Fig. 13. q_{net} (top) and k (bottom) of the reaction $CH_2CO + O \leftrightarrow CH_2 + CO_2$. Same legend as Fig.12, supplemented with — · — [42].

specific rate of Hidaka et al. [42] evaluated at 1050 K. As shown in Fig.13, the upper bound of optimization yields a specific rate description similar to the higher uncertainty limit specified in [22].

uncertainty limits suggested in [23, 34] are used to determine $1/f_{i,low} = 0.8482$ and $f_{i,high} = 8.482$.

Through the optimization, the ratio of the specific rates of the reactions $CH_2 + O_2 \leftrightarrow CO + OH + H$ and $CH_2 + O_2 \leftrightarrow CO_2 + H_2$ remains unchanged. That is, the branching between the product channels is not modified, and this requires the same multiplier to apply to the pre-exponential factor of both reactions. Practically, only eight active parameters are adjusted, while the specific rates of nine reactions are modified.

Reaction $CH_2CO + O \leftrightarrow CH_2 + CO_2$ The reaction $CH_2CO + O \leftrightarrow CH_2 + CO_2$ has a weak influence on $X_{CH,peak}$ (see Fig.1). However, its rate description is plagued by a significant uncertainty [22], which justifies its inclusion in the optimization. As shown in Fig.13, the GRI, USC, NUIG1 and NUIG2 mechanisms, and the model from the CRECK modeling group [31] are in fair agreement with the rate description recommended in [22] for $T < 1000$ K. In contrast, at the high temperatures where the reaction mostly proceeds, the specific rate included in the SD mechanism is consistent with the ketone oxidation mechanism prepared by Hidaka et al. [42] to model their shock tube experiments. The lower bound of optimization, $1/f_{i,low} = 5.808 \cdot 10^{-03}$, is adjusted to the lower limit of uncertainty of Baulch et al. [22] at 1000 K, while the upper bound, $f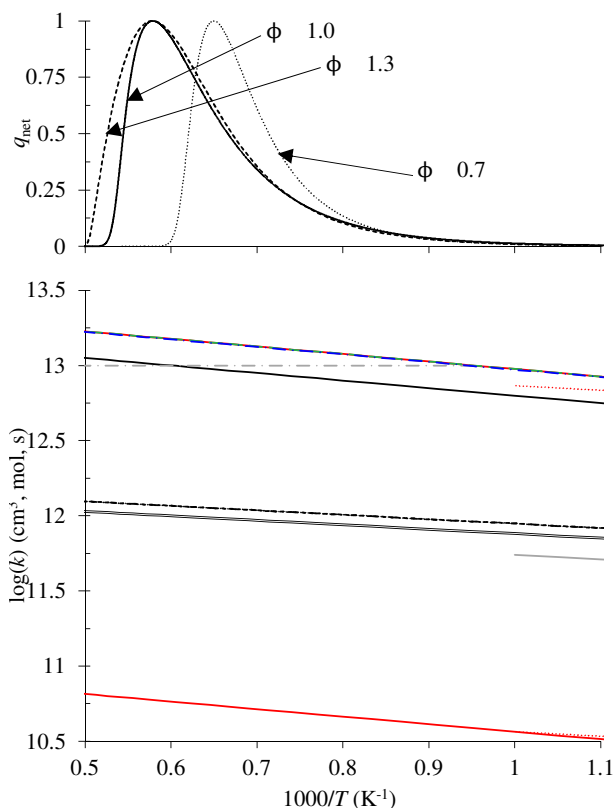_{i,high} = 1.502$, is set to the